Time Lapse seismic imaging with L1 regularization and steering filters

Yinbin Ma, Musa Maharramov, Robert Clapp and Biondo Biondi

ABSTRACT

We propose a new L1-regularized simultaneous time-lapse linearized waveform inversion method. We test the proposed method on models exhibiting production induced reservoir compaction and overburden dialation. We demonstrate that L1 regularization and steering filters significantly improve image quality in the presence of acquisition nonrepeatability issues, such as those caused by different acquisition parameters.

INTRODUCTION

Time-lapse seismic imaging and velocity analysis are challenging in complex subsurface structures because of various repeatability issues, such as different acquisition geometries, noise in the data, and insufficient illumination under the salt (Ayeni and Biondi, 2010, 2011). In a companion paper, we showed (Ma et al., 2015) that L1 regularization with steering filters can greatly improve the quality of inversion in areas of poor illumination. In this paper, we apply this technique to time-lapse seismic imaging.

First, we implement the acoustic wave equation and Born modeling for constant density, and set up four-dimensional (4D) seismic imaging as an optimization problem. It is known that the adjoint state method is an efficient way to compute the gradient for partial-differential-equation (PDE) constrained optimization. This paper is limited to the study of linearized waveform inversion, therefore the adjoint operators can be written explicitly. Both forward and adjoint operators are expressed in matrix form, confirming the conclusion from the adjoint state method.

A simple synthetic model is used to test our codes. We take a shallow part from Sigbee2A model away from the salt. The velocity is perturbed near the sea bottom and used as monitor velocity model. Numerical results show that L1 regularization is able to recover clean 4D signals. The algorithm is robust against different acquisition geometries and noise.

Our method is also tested on a synthetic model with complex subsurface structure. We construct our model from Sigbee2A model with salt body, and then, perturb the velocity in the area with poor illumination under the salt. Least squares reverse time migration (LSRTM) results suggest it is already difficult to obtain the reflectors

under the salt as can be seen in Figure 7, not to mention 4D signals. L1 regularization with steering filters is used to improve the quality of time lapse signals. We could not completely solve the time-lapse imaging problem with our method, thereby indicating the necessity to introduce geomechanical knowledge in the time-lapse study.

METHOD

In the first part of this section, the wave-equation operators used for seismic imaging are derived. In the second part, we show the objective function and optimization strategies incorporating L1 regularization with steering filters.

Acoustic wave equation and Born modeling for constant density media

We start with the wave equation from Tarantola (1984) as follows:

$$[\frac{1}{K(\mathbf{r})}\frac{\partial^2}{\partial t^2} - \nabla\left(\frac{1}{\rho}\nabla\right)]\mathbf{u}(\mathbf{r},t) = f(\mathbf{r},t), \tag{1}$$

where $K(\mathbf{r})$ is the bulk modulus, ρ is the density and $u(\mathbf{r},t)$ is the pressure field and $f(\mathbf{r},t)$ is the source function. In this paper, we assume constant density in our numerical examples, and we have $v^2 = K/\rho$. The wave equation can be simplified as:

$$[\partial_t^2 - v^2(r)\Delta]\mathbf{u}(\mathbf{r},t) = s(\mathbf{r},t), \tag{2}$$

where we define $s(\mathbf{r},t) \equiv v(\mathbf{r})^2 f(\mathbf{r},t)$.

In a seismic imaging problem, we want to find the velocity perturbation, namely the difference between the true velocity (stratigraphic velocity) and migration velocity (smooth velocity). For constant density media, there is direct relationship between velocity perturbation and acoustic reflectivity. Assuming the true velocity to be $v(\mathbf{r})$ and the smooth velocity used for migration/inversion to be $v_0(\mathbf{r})$, two different solutions can be obtained for each velocity using equation (1):

$$\begin{aligned} [\partial_t^2 - v^2(\mathbf{r})\Delta]\mathbf{u}_{\text{true}}(\mathbf{r},t) &= s(\mathbf{r},t) & (3)\\ [\partial_t^2 - v_0^2(\mathbf{r})\Delta]\mathbf{u_0}(\mathbf{r},t) &= s(\mathbf{r},t). & (4) \end{aligned}$$

Substract equation (4) from equation (4), we can get:

$$[\partial_t^2 - v_0^2(\mathbf{r})\Delta]\mathbf{u}(\mathbf{r},t) = \mathbf{m}(\mathbf{r})\partial_t^2\mathbf{u_0}(\mathbf{r},t), \tag{5}$$

where we define $\mathbf{u} \equiv \mathbf{u}_{\text{true}} - \mathbf{u_0}$, $\mathbf{m}(\mathbf{r}) = -2\delta v(\mathbf{r})/v(\mathbf{r})$ and $\delta v(\mathbf{r}) = v(\mathbf{r}) - v_0(\mathbf{r})$.

To set up an inverse problem, both the forward and adjoint of modeling operators are needed. Based on the adjoint state method, the forward operator can be written as:

$$\begin{cases} \mathbf{u}(\mathbf{r},0) & = 0 \\ \partial_t \mathbf{u}(\mathbf{r},0) & = 0 \\ (\partial_t^2 - v_0(\mathbf{r})^2\Delta)\mathbf{u}(\mathbf{r},t) & = s(\mathbf{r},t), \end{cases} \tag{6}$$

and the corresponding adjoint operator is:

$$\begin{cases} \mathbf{u}(\mathbf{r},T) & = 0 \\ \partial_t \mathbf{u}(\mathbf{r},T) & = 0 \\ (\partial_t^2 - v(\mathbf{r})^2\Delta)^\dagger \mathbf{u}(\mathbf{r},t) & = s(\mathbf{r},t). \end{cases} \tag{7}$$

The forward and adjoint operators for nonlinear modeling with varying density are computed in **Appendix A**, which allows us to extend our work to velocity estimation in the near future. The Born modeling operator in matrix form is derived in **Appendix B**, which serves as pseudocode for the numerical examples in this paper.

Joint inversion with steering filters and L1 regularization

Fixing the migration velocity $v_0(\mathbf{r})$, the data recorded at surface $\mathbf{d}$ is a linear function of $\mathbf{m}(\mathbf{r})$, as can be seen from equation (5). We use $\mathbf{L}$ to represent the linear mapping,

$$\mathbf{L}\mathbf{m} = \mathbf{d}. \tag{8}$$

In the following of the paper, we use subscripts b and m to denote baseline and monitor, respectively. Data for baseline $\mathbf{d}_b$ and monitor $\mathbf{d}_m$ are collected using true velocity model. Reverse time migration (RTM) is used to obtain images $\mathbf{m}_b^{\text{RTM}}$ and $\mathbf{m}_b^{\text{RTM}}$ as initial guess for inversion. We do an inversion for baseline and monitor separately as a first step using the following objective function,

$$\begin{aligned} \mathbf{J}_1(\mathbf{m}_b, \mathbf{m}_m) &= \frac{1}{2}||\mathbf{L}_b\mathbf{m}_b - \mathbf{d}_b||_2^2 + \frac{1}{2}||\mathbf{L}_m\mathbf{m}_m - \mathbf{d}_m||_2^2 & (9) \\ &+ \frac{\varepsilon}{2}||\mathbf{m}_b||_2^2 + \frac{\varepsilon}{2}||\mathbf{m}_m||_2^2, & (10) \end{aligned}$$

where $\varepsilon \to 0$ in the numerical sense to fit the data. After a fixed number of iterations, we obtain images $\mathbf{m}_b^{\text{LSRTM}}$ and $\mathbf{m}_b^{\text{LSRTM}}$. This step is crucial, because it balances the amplitude and attenuates the acquisition related artifacts in the RTM images. LSRTM images are also used to extract a prior gradient field, which is part of the joint-inversion objective function.

The final step is to resolve the time-lapse signal using the joint inversion, with

following objective function:

$$\mathbf{J}_2(\mathbf{m}_b, \mathbf{m}_m) = \frac{1}{2}||\mathbf{L}_b\mathbf{m}_b - \mathbf{d}_b||_2^2 + \frac{1}{2}||\mathbf{L}_m\mathbf{m}_m - \mathbf{d}_m||_2^2 \quad (11)$$

$$+ \frac{\alpha}{2}||\mathbf{W}(\mathbf{m}_m - \mathbf{m}_b)||_1 \quad (12)$$

$$+ \frac{\beta}{2}||\mathbf{W}(\nabla_{\mathbf{r}}(\mathbf{m}_m - \mathbf{m}_b))||_1 \quad (13)$$

$$+ \frac{\varepsilon}{2}||\mathbf{m}_b||_2^2 + \frac{\varepsilon}{2}||\mathbf{m}_m||_2^2, \quad (14)$$

where $\mathbf{W}$ is weight function and $\nabla_{\mathbf{r}}$ is the derivative perpendicular to $\mathbf{r}$. In the objective function, The terms (11) are data fitting and the terms (14) are used to fill the null space. The terms (12) promotes sparse 4D signals and further reduces acquisition related artifacts. Line (13) is the steering filter that promotes 4D signals along particular directions $\mathbf{r}$. In (Ma et al., 2015), we showed that steering filters are able to compensate illumination changes under the salt, and we proposed a method to construct a steering filter that can be used as prior information for inversion.

SYNTHETIC EXAMPLE 1

We select part of Sigbee 2A model as our true baseline velocity model. We perturb the velocity at the boundary of subsurface layers and use it as true monitor velocity model. Migration velocity is the same for both baseline and monitor. The velocity differences between true velocity and migration velocity are shown in Figure 1.

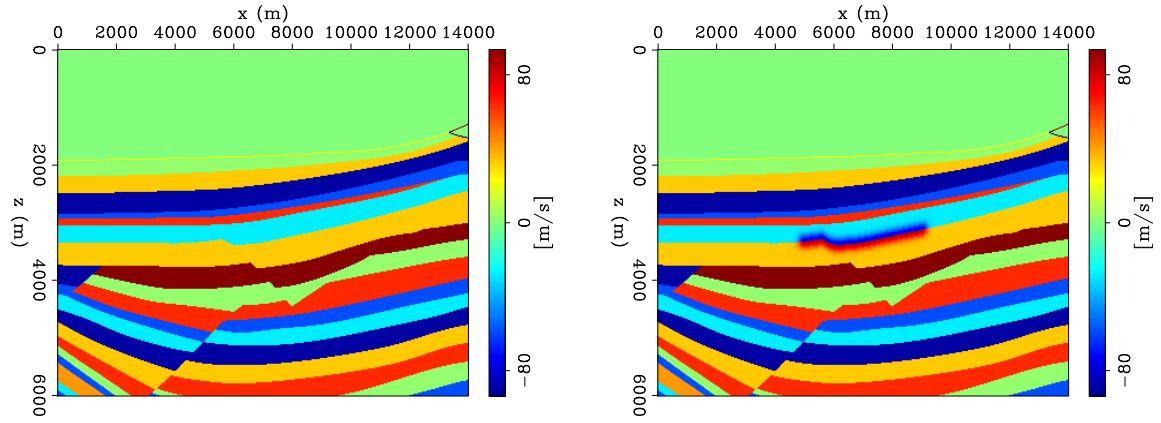

Figure 1: (a) baseline velocity perturbation. (b) monitor velocity perturbation. [**ER**]

Model size is 301×701 with 20 meters (m) between neighboring pixels. 48 sources spaced every 200 meters with up to 701 receivers spaced every 20 meters, are used to create the synthetic data. To simulate the acquisition nonreproducibility issues, we turn off receivers randomly for baseline and monitor surveys. We also assume there are 100 receivers missing in the monitor recording because of the presence of a

platform right above the reservoir. Uniform random noise is added to the data. The synthetic data can be seen in Figure 2. For one shot gather, we have 397 traces for baseline, and 224 traces for monitor.

RTM image from baseline model is used as initial guess in LSRTM step for both baseline and monitor. Figure 3 shows the LSRTM results after 500 conjugate gradient (CG) steps. The amplitude difference at the reservoir is observable at this stage. Substracting the two images, as seen in Figure 4(a), we get very noisy results contaminated by footprints from the acquisition gap in the monitor survey. Nevertheless, the time-lapse signal can be interpreted.

Simultaneous joint inversion is then solved using iteratively reweighted least squares (IRLS) for 20 by 10 CG steps, and the results are shown in Figure 4(b). Weight function $\mathbf{W}$ has non-zero values in a rectangle around the area with production induced velocity change. Because of the simplicity of the model, $\nabla_{\mathbf{r}} = \nabla_{\mathbf{x}}$ would be sufficient. In this example, 4D signals with L1 regularization can be recovered.

SYNTHETIC EXAMPLE 2

In this section, the target area is selected under the salt. Because of the complexity, we add acquisition nonrepeatability issues gradually to identify the boundary of failure and success. The first subsection shows results with different acquisition geometries. The second subsection shows results with an additional acquisition gap in the monitor.

The true velocity models for baseline and monitor are constructed from part of the Sigbee 2A model with salt. Model size is 301×501 with 20 meters (m) between neighboring pixels. 48 sources spaced every 180 meters with up to 501 receivers spaced every 20 meters, are used to create the synthetic data. Migration velocity is the same for both baseline and monitor. The velocity differences between true velocity and migration velocity are shown in Figure 5. Two reservoirs are included in our model, one in the relatively easy part and another one under the salt.

Subsalt 4D imaging with different acquisition geometry

Each shot gather contains 383 traces for the baseline and 330 traces for the monitor. Two shot gathers are shown in Figure 6, from baseline and monitor survey seperately. RTM images from baseline and monitor are created seperately and used as initial guesses for LSRTM. Images from LSRTM in Figure 7 are computed after 200 CG steps. The predicted 4D signals are shown in Figure 8(a).

From the LSRTM results, a smooth gradient field is constructed using the method in Ma et al. (2015), and used as prior information for the joint inversion.

Finally, we solve the joint inversion problem using IRLS for 20 by 10 iterations, and the result can be seen in Figure 8(b).

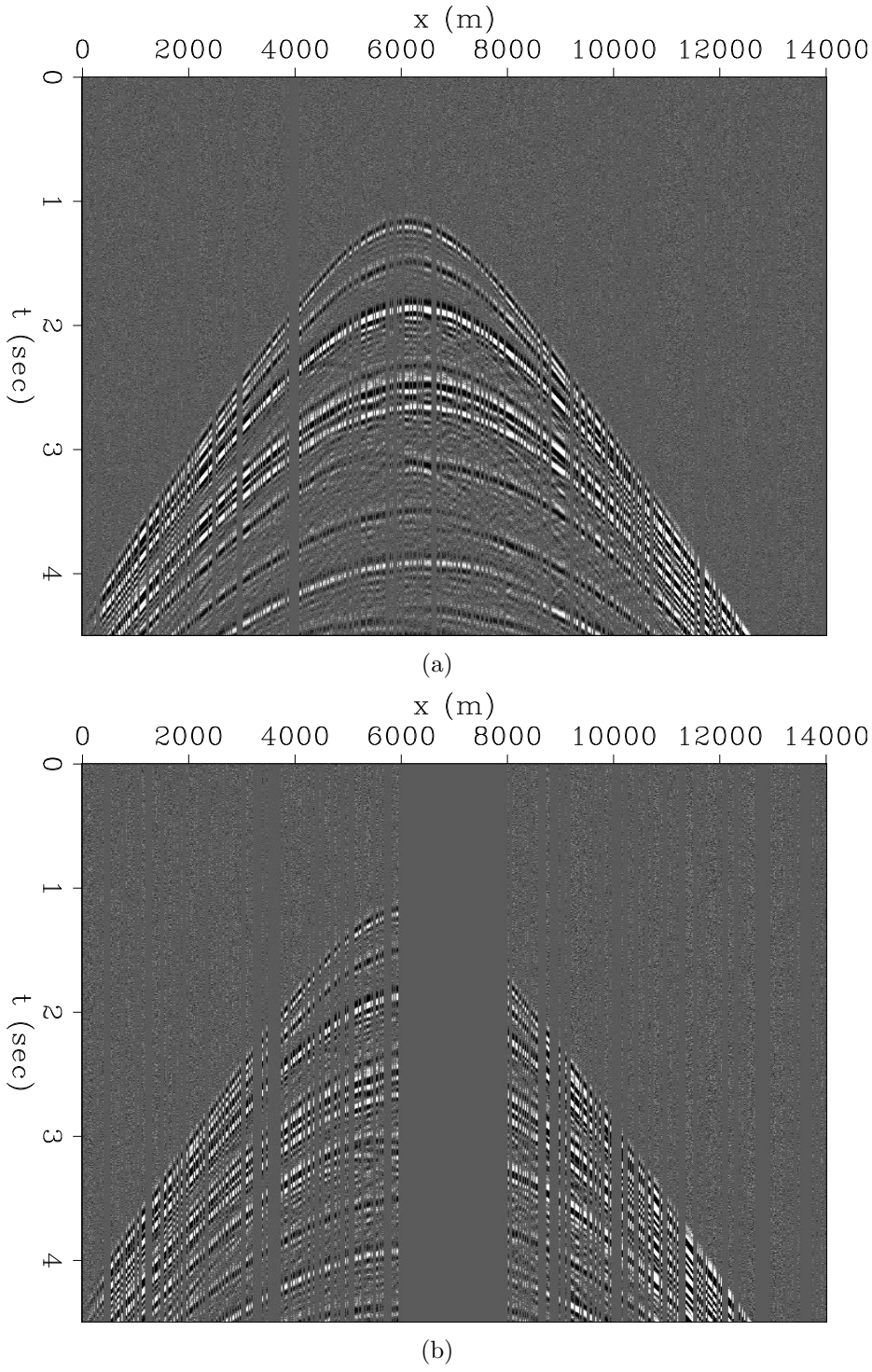

Figure 2: (a) baseline shot gather. (b) monitor shot gather. (same percentile clip) [**CR**]

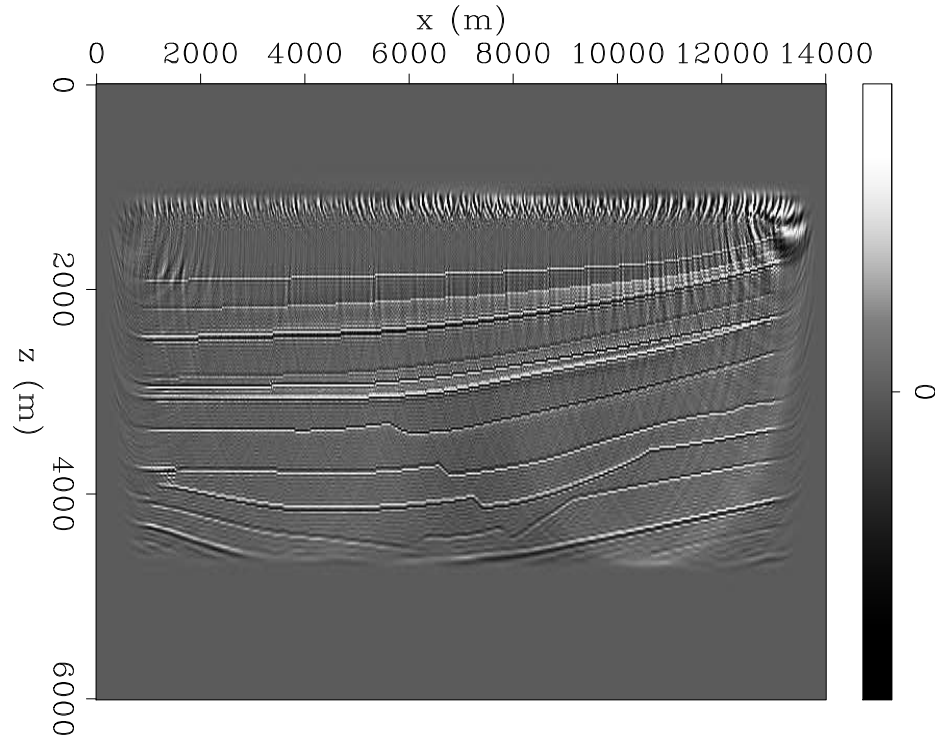

(a)

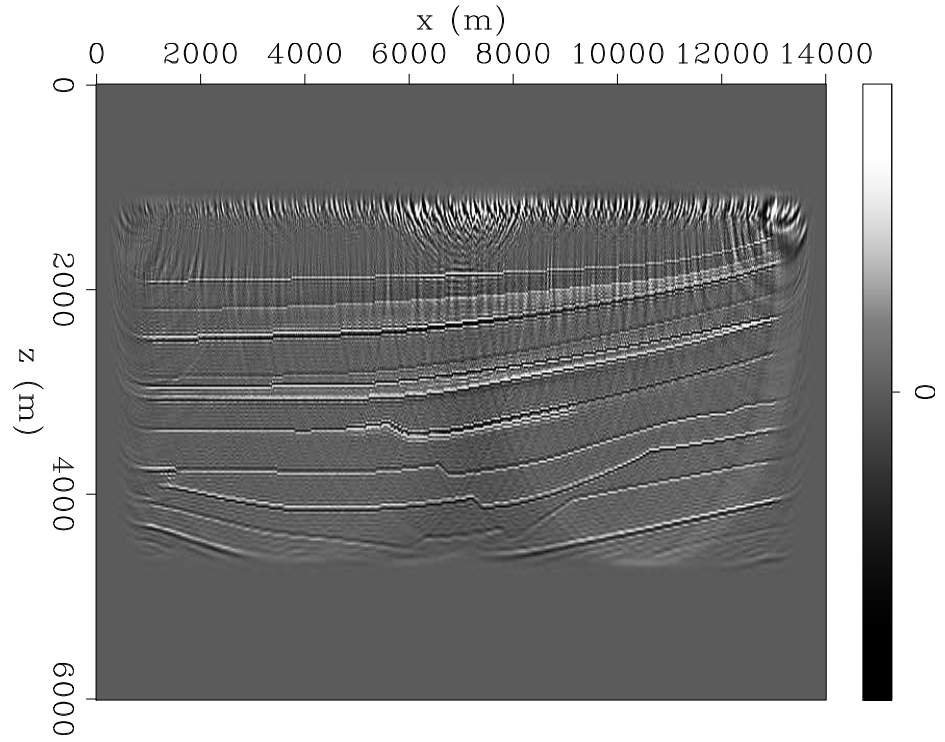

(b)

Figure 3: (a) baseline image from LSRTM. (b) monitor image from LSRTM. (same percentile clip) [**CR**]

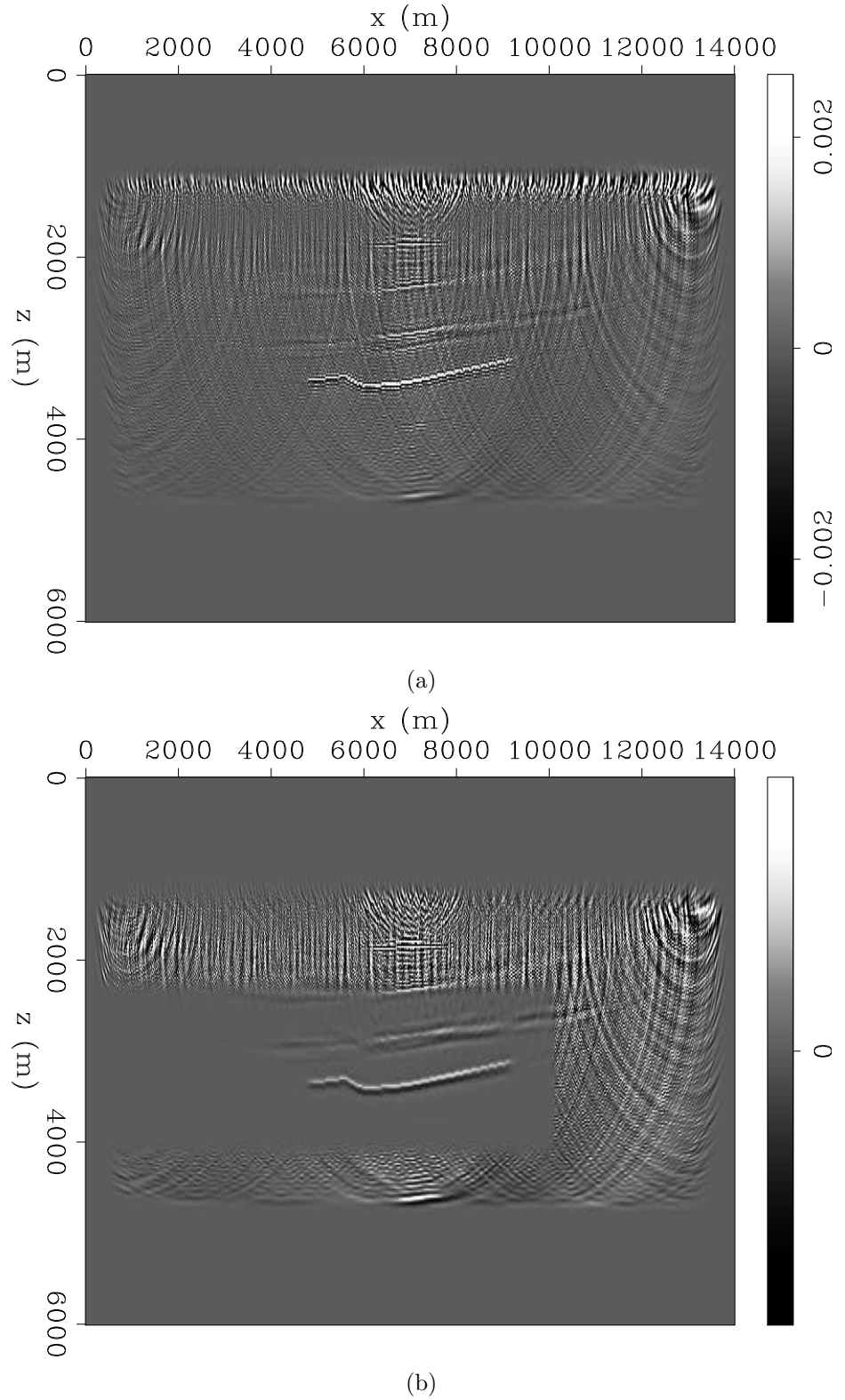

Figure 4: (a) difference bewteen baseline and monitor images from LSRTM. (b) difference between baseline and monitor from Joint IRLS. The clean rectangle in the middle is where $\mathbf{W}(\mathbf{r}) \neq 0$. [**CR**]

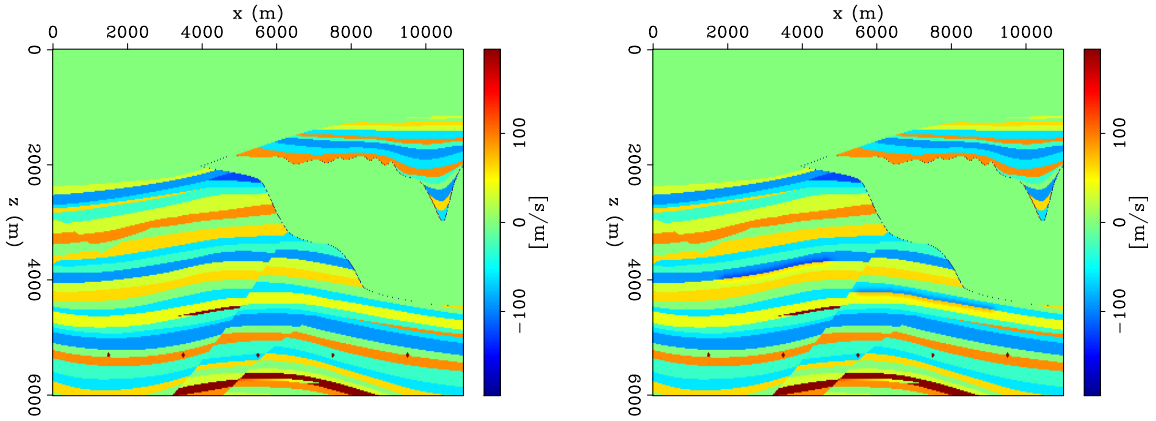

(a) (b)

Figure 5: Left: baseline velocity perturbation; right: monitor velocity perturbation. [**ER**]

Subsalt 4D imaging with different acquisition geometry and acquisition gap

50 receivers are removed from the monitor survey to create an acquisition gap. Two shot gathers are shown in Figure 9. RTM images from baseline and monitor are created seperately and used as initial guesses for LSRTM. Images from LSRTM in Figure 10 are computed after 200 CG steps. The predicted 4D signals are shown in Figure 11(a). The acquisition gap leads to a incorrect prediction of 4D signals under the salt. Around $x = 5000m$, LSRTM results suggest there are reflectivity changes both above and below the true velocity perturbation, near $z = 3000m$ and $z = 5000m$.

We then solve the joint inversion problem using IRLS for 20 by 10 iterations, and the result can be seen in Figure 11(b). The incorrect prediction of 4D signals is not completely removed from the joint inversion with steering filters, maybe because they are in the null space of steering filter and forward modeling operator $\mathbf{L}$. The limitation of steering filters indicates that more sophisticated regularization terms are necessary in time-lapse study.

CONCLUSIONS AND FUTURE WORK

We applied L1 regularization and steering filters to the time-lapse imaging problem. Our numerical results suggest great improvements can be achieved when the subsurface structure is relatively simple. We also demonstrated enhancement of 4D signals under the salt can be achieved. The methods in this paper extract information purely from the seismic data. Subsalt imaging is still challenging when reliable data is not present. The bright side is that in 4D we have additional data from reservoir simu-

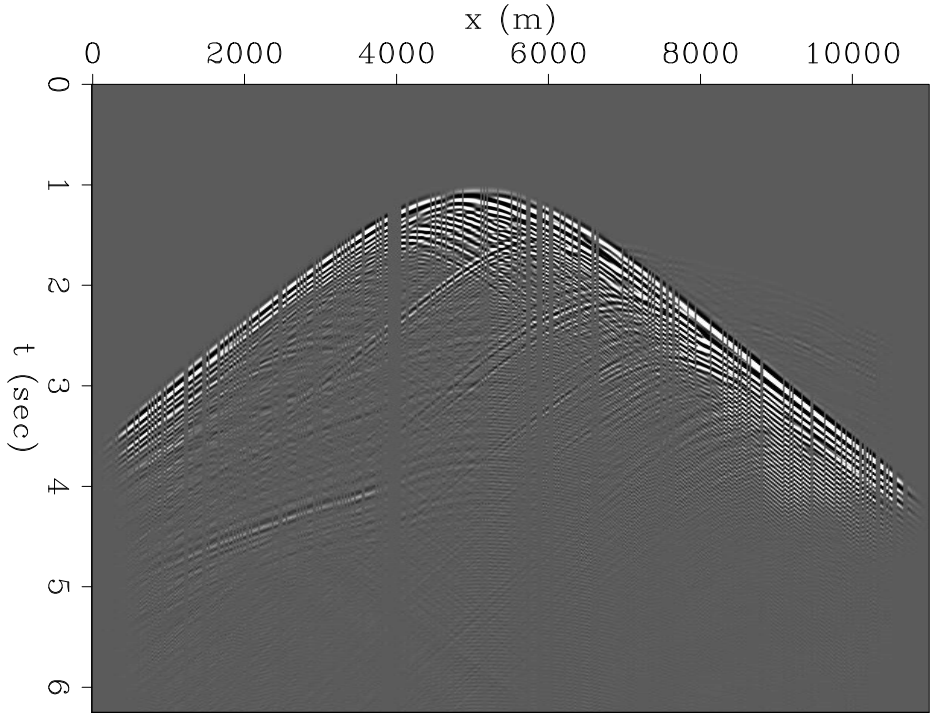

(a)

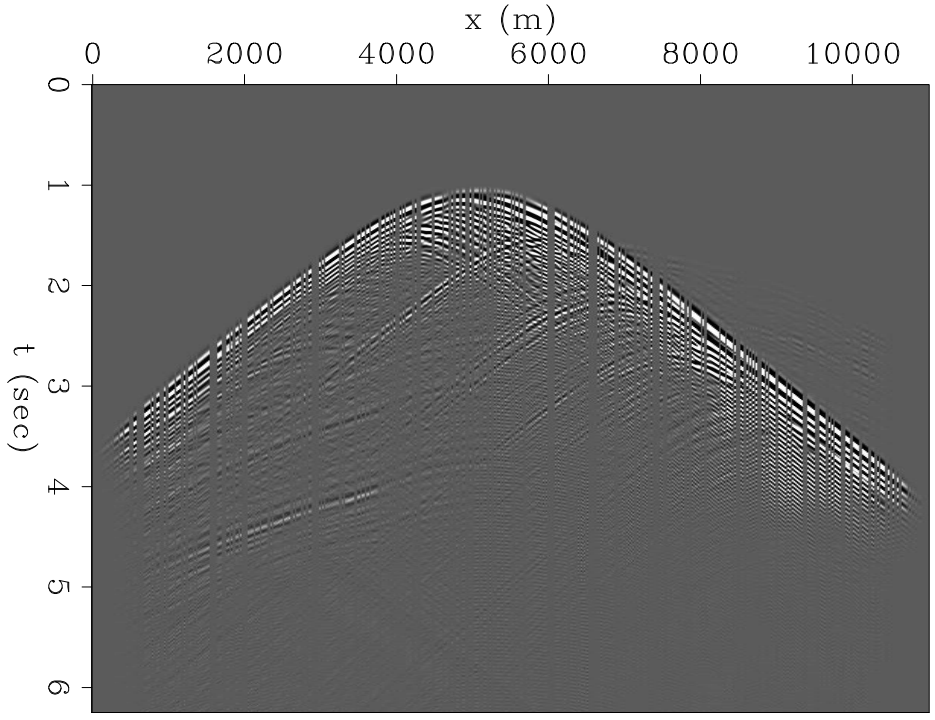

(b)

Figure 6: (a) baseline shot gather. (b) monitor shot gather. (same percentile clip) [**CR**]

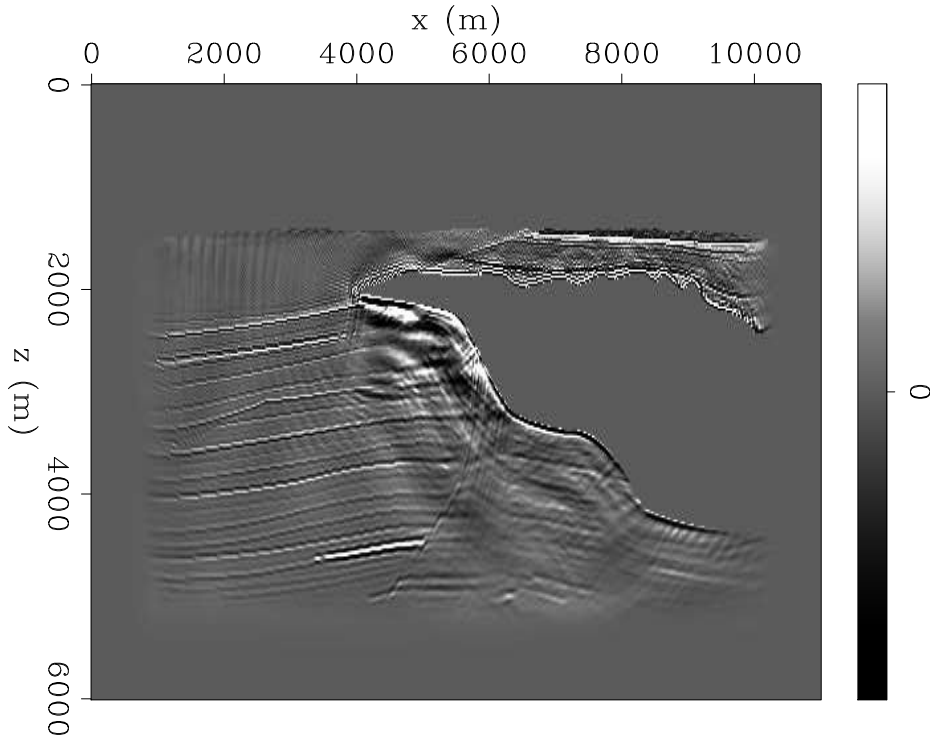

(a)

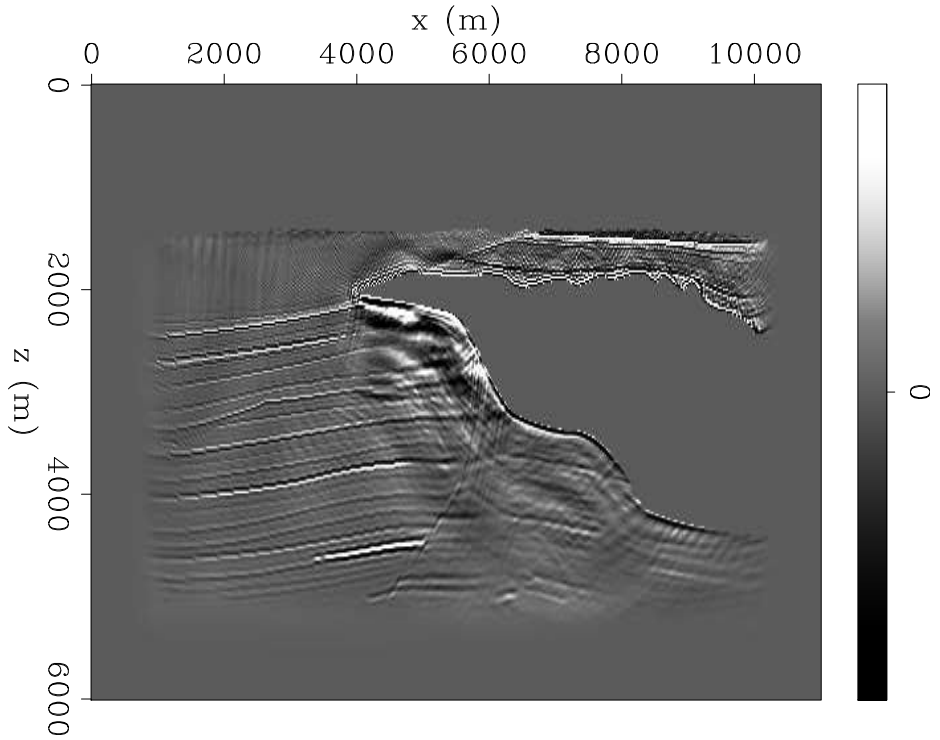

(b)

Figure 7: (a) baseline image from LSRTM. (b) monitor image from LSRTM. (same percentile clip) [**CR**]

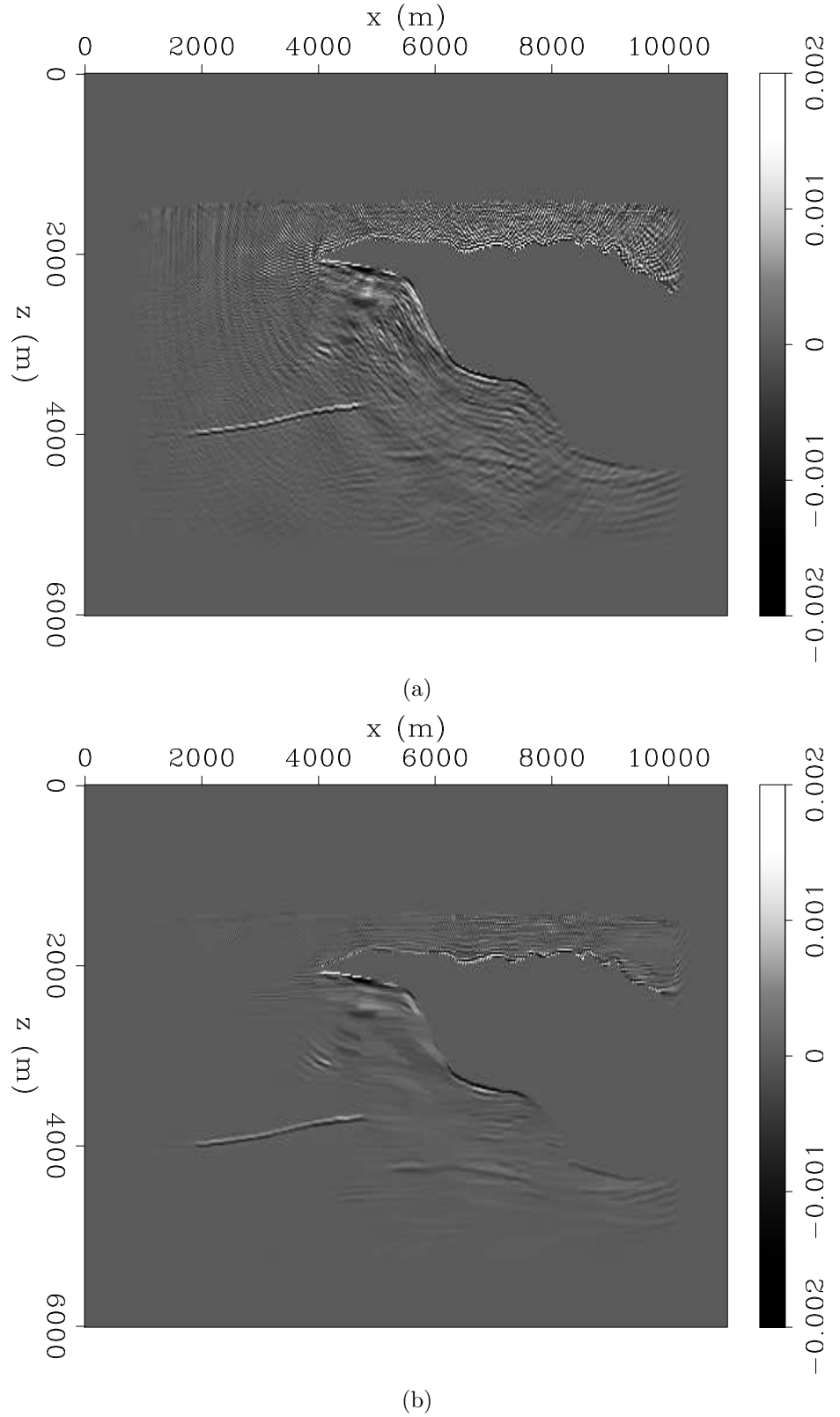

Figure 8: (a) difference bewteen baseline and monitor images from LSRTM. (b) difference between baseline and monitor from Joint IRLS. [**CR**]

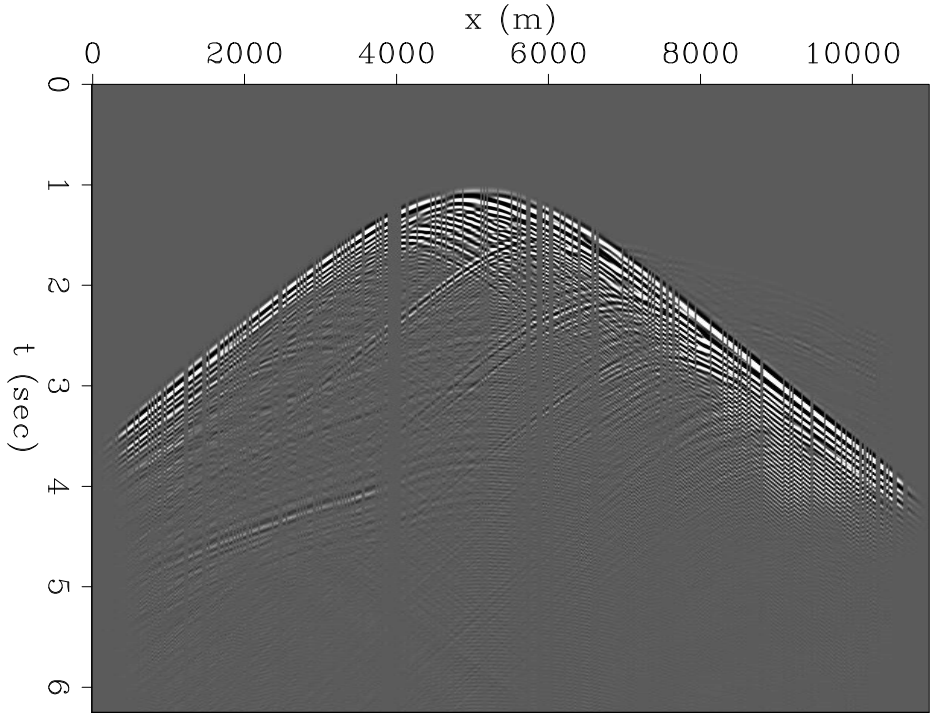

(a)

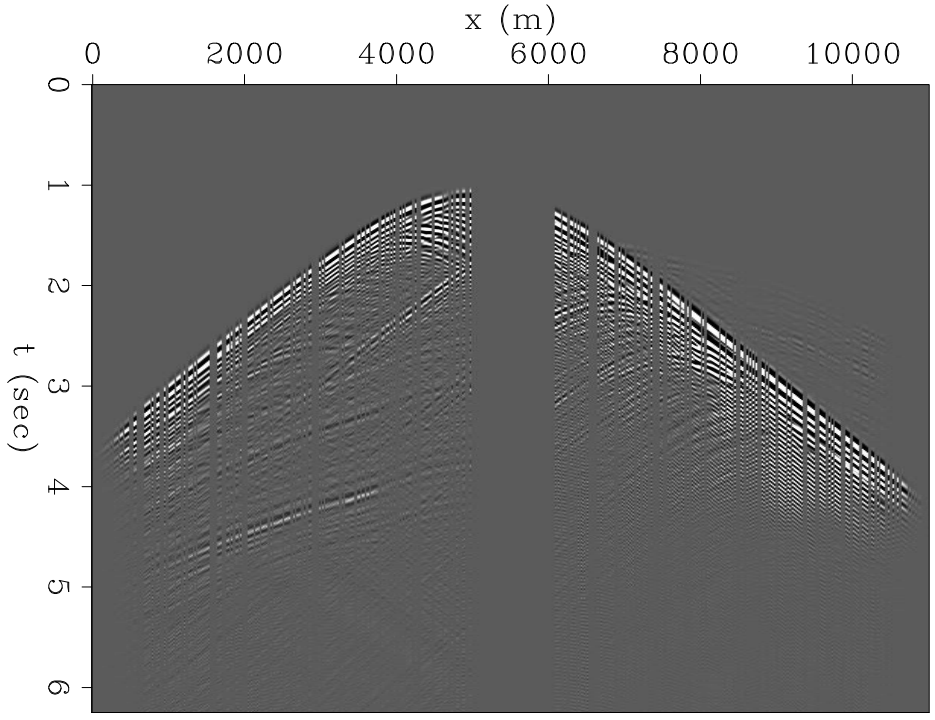

(b)

Figure 9: (a) baseline shot gather. (b) monitor shot gather. (same percentile clip) [**CR**]

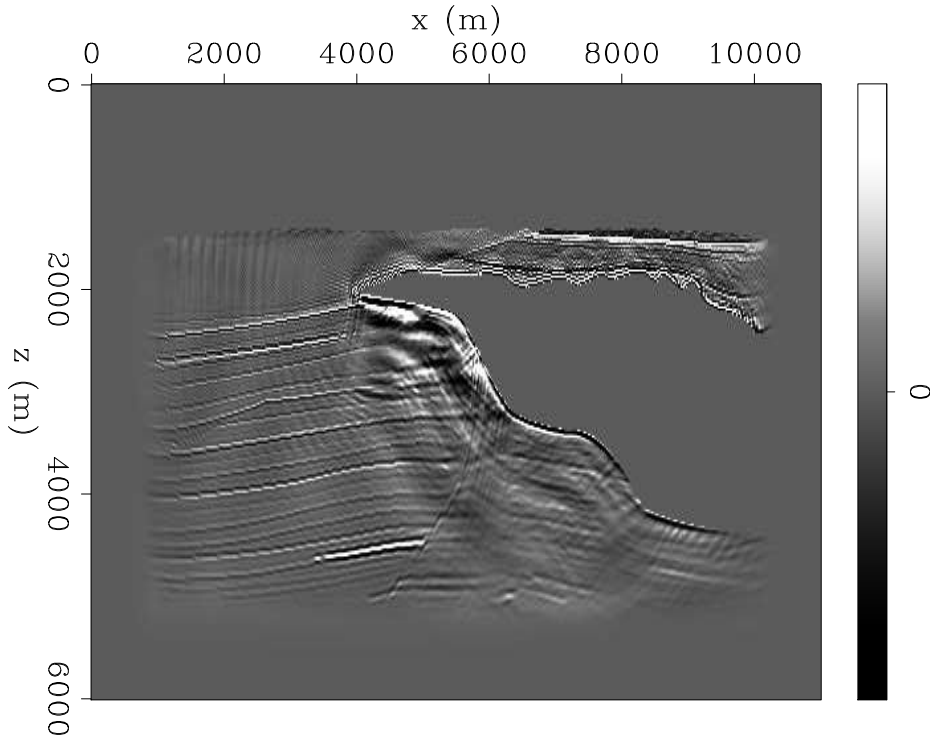

(a)

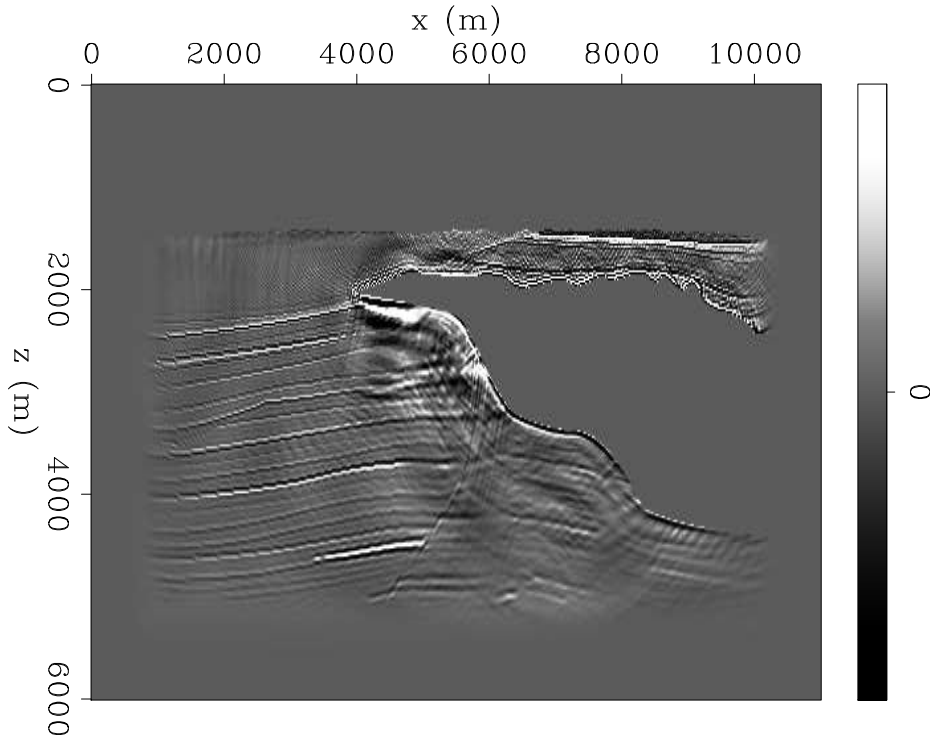

(b)

Figure 10: (a) baseline image from LSRTM. (b) monitor image from LSRTM. (same percentile clip) [**CR**]

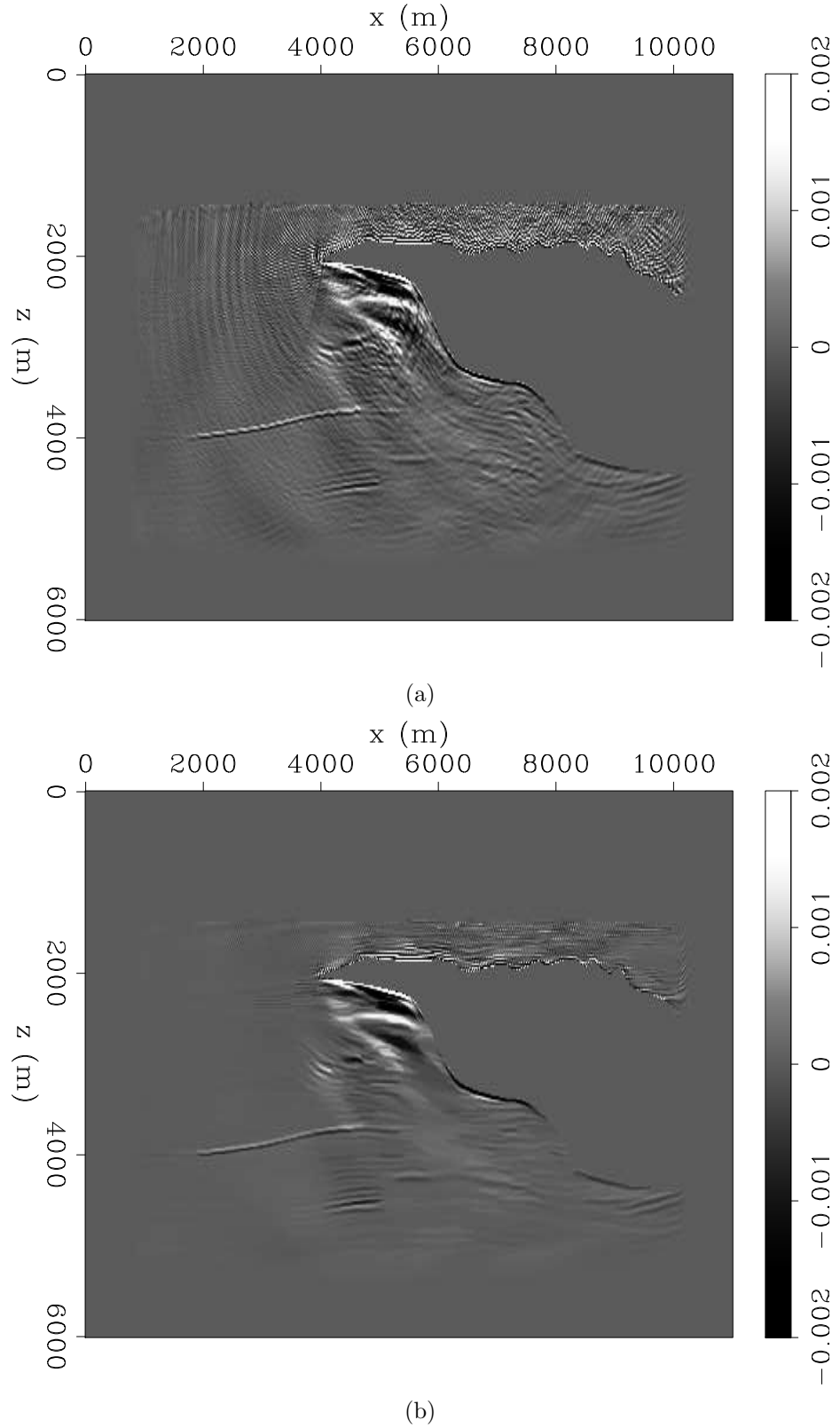

Figure 11: (a) difference bewteen baseline and monitor images from LSRTM. (b) difference between baseline and monitor from Joint IRLS. [**CR**]

lation, well logs, rock physics and geomechanics etc. In our next work, we need to bring in geomechanical information to build more robust algorithms.

ACKNOWLEDGMENTS

We would like to thank Huy Le, Gustavo Alves, Chris Leader and Stewart Levin for their valuable comments and numerious discussions.

APPENDIX A: FULL WAVEFORM INVERSION GRADIENT AND LINEARIZED VERSION

We aim at inverting velocity and density simultaneously. In this appendix, we derive the Frechet derivative of objective function for a full-waveform inversion. We follow the notations of (Liu and Tromp, 2006; Plessix, 2006; Bai and Yingst, 2014). We compute the gradient for a single-shot gather. Our objective function is:

$$J(v,\rho) = \frac{1}{2}\sum_r \int_0^T \|u(x_r,t) - d(x_r,t)\|_2^2 dt, \tag{15}$$

where $u(x_r,t)$ is a computed wavefield and $d(x_r,t)$ is recorded data. Our objective function is constrained by the following PDE:

$$\begin{cases} [\frac{1}{v^2}\partial_t^2 - \rho\nabla(\frac{1}{\rho}\nabla)]u & = f \\ u(x,0) & = 0 \\ \partial_t u(x,0) & = 0. \end{cases} \tag{16}$$

The Lagrangian:

$$\begin{aligned} L(v,\rho,\lambda,\mu_1,\mu_2) &= \frac{1}{2}\sum_r \int_0^T \|u(x_r,t) - d(x_r,t)\|_2^2 dt & (17)\\ &- \int_0^T \int \langle \lambda, \frac{1}{v^2}\partial_t^2 u - \rho\nabla(\frac{1}{\rho}\nabla u) - f\rangle d^3_\Omega x dt & (18)\\ &- \int_\Omega \langle \mu_1, u(x,0)\rangle d^3x & (19)\\ &- \int_\Omega \langle \mu_2, \partial_t u(x,0)\rangle d^3x. & (20) \end{aligned}$$

Perturb Lagrangian and we can get:

$$\begin{aligned} \delta L &= \sum_r \int_0^T \int \langle u(x_r,t) - d(x_r,t), \delta u(x,t)\rangle \delta_3(x-x_r) d^3x dt & (21)\\ &- \int_0^T \int_\Omega \langle \lambda, -\frac{2}{v^3}\delta v \partial_t^2 u - \delta\rho\nabla(\frac{1}{\rho}\nabla u) + \rho\nabla(\frac{\delta\rho}{\rho^2}\nabla u) - \delta f\rangle d^3x dt & (22)\\ &- \int_0^T \int_\Omega \langle \lambda, \frac{1}{v^2}\partial_t^2 \delta u - \rho\nabla(\frac{1}{\rho}\nabla\delta u)\rangle d^3x dt & (23)\\ &- \int_\Omega \langle \mu_1, \delta u(x,0)\rangle d^3x & (24)\\ &- \int_\Omega \langle \mu_2, \partial_t \delta u(x,0)\rangle d^3x. & (25) \end{aligned}$$

Before we go further, we want to briefly mention the effects of each term in the previous equation. Line (22) is used to derive the Frechet derivative. Line (21) and (23) form another PDE by properly choosing the Lagrangian multipliers, which are used in the computation of gradient. Line (24) and (25) vanish with proper μ_1 and μ_2.

We will first derive the PDE constraints for λ. Define A to be the sum of line (23), (24), and (25) of δL,

$$\begin{aligned} A &= -\int_0^T \int_\Omega \langle \lambda, \frac{1}{v^2}\partial_t^2 \delta u - \rho \nabla (\frac{1}{\rho}\nabla \delta u)\rangle d^3x dt \qquad (26)\\ &= -\int_\Omega \langle \mu_1, \delta u(x,0)\rangle d^3x - \int_\Omega \langle \mu_2, \partial_t \delta u(x,0)\rangle d^3x \\ &= -\int_0^T \int_\Omega \langle \frac{1}{v^2}\partial_t \lambda - \nabla^\dagger(\frac{1}{\rho}\nabla^\dagger(\rho\lambda)), \delta u\rangle d^3x dt \\ &\quad -\int_\Omega \langle \mu_2 - \frac{1}{v^2}\lambda, \partial_t \delta u(x,0)\rangle d^3x - \int_\Omega \langle \mu_1 + \frac{1}{v^2}\partial_t\lambda, \delta u(x,0)\rangle d^3x \\ &\quad -\int_\Omega \langle \lambda, \frac{1}{v^2}\partial_t \delta u(x,T)\rangle d^3x \\ &\quad -\int_\Omega \langle -\partial_t\lambda, \frac{1}{v^2}\delta u(x,T)\rangle d^3x. \end{aligned}$$

We can choose $\mu_2 = \frac{1}{v^2}\lambda$, $\mu_1 = -\frac{1}{v^2}\partial_t\lambda$ to simplify the previous equation. Define B to be the sum of line 22 of δL, assuming $\delta f = 0$ and proper boundary condition, we get:

$$\begin{aligned} B &= -\int_0^T \int_\Omega \langle \lambda, -\frac{2}{v^3}\delta v \partial_t^2 u - \delta\rho\nabla(\frac{1}{\rho}\nabla u) + \rho\nabla(\frac{\delta\rho}{\rho^2}\nabla u) - \delta f\rangle d^3x dt \qquad (27)\\ &= \int_0^T \int_\Omega \langle \lambda, \frac{2}{v^3}\partial_t^2 u\rangle \delta v d^3x dt \\ &\quad \int_0^T \int_\Omega \langle \lambda, \frac{1}{\rho}(\nabla\rho)(\nabla u)\rangle \delta\rho d^3x dt. \end{aligned}$$

Substitute A and B back into δL,

$$
\begin{aligned}
\delta L &= \int_0^T \int_\Omega \langle \lambda, \frac{2}{v^3}\partial_t^2 u\rangle \delta v d^3x dt \\
&\int_0^T \int_\Omega \langle \lambda, \frac{1}{\rho}(\nabla\rho)(\nabla u)\rangle \delta\rho d^3x dt \\
&- \int_0^T \int_\Omega \langle \frac{1}{v^2}\partial_t\lambda - \nabla^\dagger(\frac{1}{\rho}\nabla^\dagger(\rho\lambda)) - \sum_r (u(x_r,t)-d(x_r,t))\delta_3(x-x_r), \delta u(x,t)\rangle d^3x dt \\
&- \int_\Omega \langle \lambda, \frac{1}{v^2}\partial_t \delta u(x,T)\rangle d^3x \\
&- \int_\Omega \langle -\partial_t\lambda, \frac{1}{v^2}\delta u(x,T)\rangle d^3x.
\end{aligned} \tag{28}
$$

Choose the λ such that the last three lines vanish, and we get the gradients,

$$
\begin{cases}
\frac{\partial J}{\partial v} &= \int_0^T \int_\Omega \langle \lambda, \frac{2}{v^3}\partial_t^2 u\rangle d^3x dt \\
\frac{\partial J}{\partial \rho} &= \int_0^T \int_\Omega \langle \lambda, \frac{1}{\rho}(\nabla\rho)(\nabla u)\rangle d^3x dt,
\end{cases} \tag{29}
$$

subject to:

$$
\begin{cases}
\frac{1}{v^2}\partial_t\lambda - \nabla^\dagger(\frac{1}{\rho}\nabla^\dagger(\rho\lambda)) &= \sum_r (u(x_r,t)-d(x_r,t))\delta_3(x-x_r) \\
\lambda(x,T) &= 0 \\
\partial_t\lambda(x,T) &= 0.
\end{cases} \tag{30}
$$

λ satisfies the adjoint of wave equation, and we emphasize that $\nabla^\dagger \neq \nabla$.

In this paper, we only need linearized waveform inversion with constant density, and we can simplify the gradient expression:

$$
\frac{\partial J}{\partial v} = \int_0^T \int_\Omega \langle \lambda, \frac{2}{v^3}\partial_t^2 u\rangle d^3x dt \tag{31}
$$

$$
\frac{1}{v^2}\partial_t\lambda - (\nabla^\dagger)^2\lambda = \sum_r (u(x_r,t)-d(x_r,t))\delta_3(x-x_r) \tag{32}
$$

$$
\lambda(x,T) = 0 \tag{33}
$$

$$
\partial_t\lambda(x,T) = 0 \tag{34}
$$

$$
\rho(x) = \rho_0. \tag{35}
$$

APPENDIX B: UNDERSTANDING FORWARD/ADJOINT OF WAVE PROPAGATION IN MATRIX FORM

In this section, Born modeling for constant density in matrix form is derived, following the idea of (Ji, 2009; Almomin, 2013) . All the necessary modules are included and they should be ready to translate into real code.

We discrete time into $[0, \Delta t, 2\Delta t, \cdots, N\Delta t]$, with $T = N\Delta t$. Assume we have obtained the wavefield $\tilde{u}(x,t)$ for $t = 0, \Delta t, \cdots, N\Delta t$, we can then approximate $\partial_t^2 u_0(x,t)$ for $t = 0, \Delta t, \cdots, (N-1)\Delta t$, using a second order finite difference.

Use u^i to represent the wavefield at $t = i \times \Delta t$, and use $U = [u^0, u^1, \cdots, u^N]^T \in \mathbb{R}^{N \times dom}$ to represent wavefield at the domain in which we are interested. First, we need to create the source term $S = [s^0, s^1, \cdots, s^{N-1}, s^N = 0]^T$, it can be described as:

$$S = BVm, \tag{36}$$

where $B = [D_t^2 u^0, D_t^2 u^1, \cdots, D_t^2 u^{N-1}, 0]^T$, and $V = v(r)^2$. D_t^2 is 2nd order finite difference operator.

An implicit trick we want to impose is a shift operator T_1 with the effect:

$$T_1 S = T_1 \begin{bmatrix} s^0 \\ s^1 \\ \vdots \\ s^{N-1} \\ s^N = 0 \end{bmatrix} = \begin{bmatrix} 0 \\ s^0 \\ s^1 \\ \vdots \\ s^{N-1} \end{bmatrix}. \tag{37}$$

We need this operator to compute $u_1, \cdots, u_N$; and we need $s_0, \cdots, s_{N-1}$, and the shift operator to simplify the following expression. It is also important to obtain the correct final state for the adjoint operator.

The explicit form for time marching is:

$$u^{t+1} = (2 - \frac{\Delta t^2}{\Delta x^2} v^2 \Delta) u^t - u^{t-1} + s^t. \tag{38}$$

After the source wavefield is obtained, we claim the following operator is time marching:

$$M_t \equiv \begin{bmatrix} I_{(t-1)\times(t-1)} & 0 & 0 \\ 0 & A_{3\times 3} & 0 \\ 0 & 0 & I_{(N-t-2)\times(N-t-2)} \end{bmatrix}. \tag{39}$$

which maps $[u^0, \cdots, u^t, s^t, \cdots, s^{N-1}]^T$ to $[u^0, \cdots, u^t, u^{t+1}, s^{t+1}, \cdots, s^{N-1}]$. The time marching kernel:

$$A = \begin{bmatrix} I & 0 & 0 \\ 0 & I & 0 \\ -P & PT & P \end{bmatrix} \tag{40}$$

$$T = 2 - \frac{\Delta t^2}{\Delta x^2} v^2 \Delta, \tag{41}$$

with P as absorbing boundary operator. The effect of M_t can be checked by induction, and the boundary term need some attention.

Now, we have:

$$M_{N-1} M_{N-2} \cdots M_0 T_1 B V m = U = \begin{bmatrix} u^0 = 0 \\ u^1 \\ \vdots \\ u^{N-1} \\ u^N \end{bmatrix}. \tag{42}$$

Thus, it is obvious that $M_{N-1} M_{N-2} \cdots M_0 T_1 B V$ is the forward operator for Born modeling.

It is interesting to see the exact adjoint of this method:

$$T_1^T M_0^T \cdots M_{N-1}^T \begin{bmatrix} u^0 \\ u^1 \\ \vdots \\ u^{N-1} \\ u^N \end{bmatrix} = T_1^T \begin{bmatrix} s^0 = \text{weird state} \\ s^1 \\ \vdots \\ s^{N-1} \\ s^N \end{bmatrix} = \begin{bmatrix} \tilde{s}^0 \\ \tilde{s}^1 \\ \vdots \\ \tilde{s}^{N-1} \\ \tilde{s}^N = 0 \end{bmatrix}, \tag{43}$$

which is exactly what the adjoint formula predicts, with the correct final condition.

REFERENCES

Almomin, A., 2013, Accurate implementation of two-way wave-equation operators: SEP Report, **149**, 279–286.

Ayeni, G. and B. Biondi, 2010, Target-oriented joint least-squares migration/inversion of time-lapse seismic data sets: Geophysics, **75**, R61–R73.

———, 2011, Wave-equation inversion of time-lapse seismic data sets: SEP Report, **143**, 117–134.

Bai, J. and D. Yingst, 2014, Simultaneous inversion of velocity and density in time-domain full waveform: SEG Technical Program Expanded Abstracts 2014, 922–927.

Ji, J., 2009, An exact adjoint operation pair in time extrapolation and its application in least-squares reverse-time migration: Geophysics, **74**, H27–H33.

Liu, Q. and J. Tromp, 2006, Finite-frequency kernels based on adjoint methods: Bulletin of the Seismological Society of America, **96**, 2383–2397.

Ma, Y., M. Maharramov, R. Clapp, and B. Biondi, 2015, Illumination compensation with L1 regularization and steering filters: SEP Report, **158**.

Plessix, R. E., 2006, A review of the adjoint-state method for computing the gradient of a functional with geophysical applications: Geophysical Journal International, **167**, 495–503.

Tarantola, A., 1984, Inversion of seismic reflection data in the Acoustic Approximation: Geophysics, **49**, 1259–1266.